iScience

CellPress

Article

The Self-Passivation Mechanism in Degradation of $BiVO_4$ Photoanode

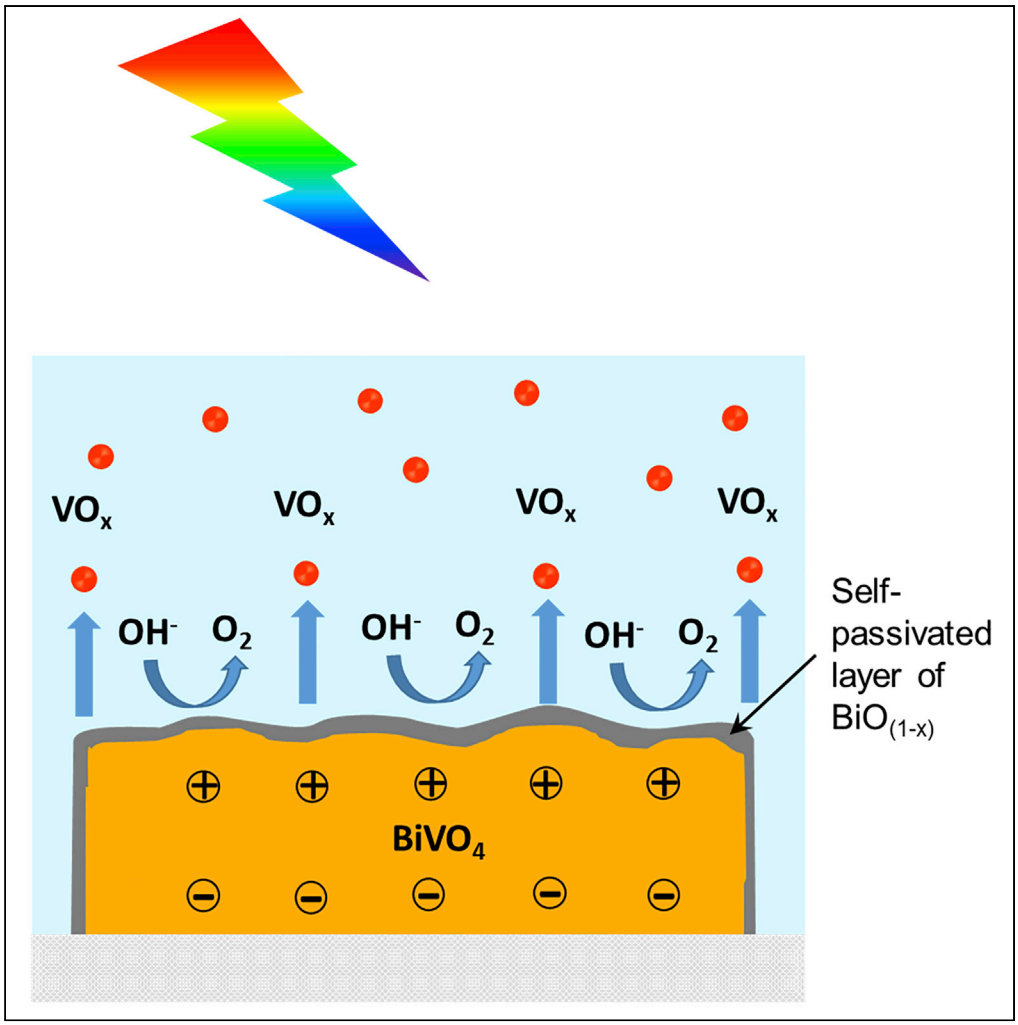

Xin Yao, Xin Zhao, Jun Hu, ..., Yizhong Huang, Zhong Chen, Thirumany Sritharan

ASZChen@ntu.edu.sg (Z.C.)
assritharan@ntu.edu.sg (T.S.)

HIGHLIGHTS

A mechanism of degradation is developed for $BiVO_4$ photoanode during photolysis

Degradation occurs by V dissolution and Bi accumulation on the anode as oxide

Accumulating Bi oxide passivates the anode

Thermodynamic modeling supports this mechanism

Yao et al., iScience 19, 976–985
September 27, 2019
https://doi.org/10.1016/j.isci.2019.08.037

iScience

CellPress

Article

The Self-Passivation Mechanism in Degradation of $BiVO_4$ Photoanode

Xin Yao,[1,2,4] Xin Zhao,[1,4] Jun Hu,[1] Huiqing Xie,[3] Danping Wang,[1,2] Xun Cao,[1] Zheng Zhang,[3] Yizhong Huang,[1] Zhong Chen,[1,2,*] and Thirumany Sritharan[1,2,5,*]

SUMMARY

$BiVO_4$ is a promising photoanode material for solar-assisted water splitting in a photoelectrochemical cell but has a propensity to degrade. Investigations carried out here in 0.1 M Na_2SO_4 electrolyte showed that degradation is by dissolution of V in the electrolyte while Bi is retained on the anode probably in the form of solid Bi oxide (Bi_2O_3, Bi_4O_7). Accumulation of Bi oxide on the anode surface leads to passivation from further degradation. Thermodynamic modeling of possible degradation reactions has provided theoretical support to this mechanism. This self-passivation is accompanied by a decrease in photocurrent density, but it protects the anode against extensive photocorrosion and contributes to long-term stability. This is a more definitive understanding of degradation of $BiVO_4$ during water splitting in a photoelectrochemical cell. This understanding is imperative for both fundamental and applied research.

INTRODUCTION

Artificial photosynthesis, which captures and stores solar energy in the chemical bonds of a fuel, is a potential solution to the energy storage problem (Barber, 2009). Solar-assisted water splitting to produce hydrogen fuel has received significant research interest in this regard (Gust et al., 2009; Lewis and Nocera, 2006; Maeda and Domen, 2010; Sivula and van de Krol, 2016). The photoelectrochemical cell (PEC) is a versatile tool for photolysis of water where a semiconductor is used to harvest solar energy and an external bias is applied to facilitate the water splitting reactions (Blankenship et al., 2011; Grätzel, 2001; Li et al., 2013; Walter et al., 2010). Such electrochemical water photolysis was first reported by Fujima and Honda using a TiO_2 (band gap = 3.0–3.2 eV) photoanode (Fujishima and Honda, 1972). For more efficient photolysis, a narrower bandgap and a valence band edge above 2.0 eV versus reversible hydrogen electrode (RHE) is mandatory to provide sufficient overpotential for holes to oxidize water at the anode. Simultaneously, a negative conduction band edge is required at the cathode for electrons to reduce water. The efficiency of light absorption is principally determined by the bandgap of the semiconductor, which is the basis of theoretical calculations of solar to hydrogen conversion efficiency. The bandgap is also a measure of the stability of a compound, and thus semiconductors with narrow bandgaps are usually vulnerable to degradation in photoelectrodes (Grätzel, 2001).

$BiVO_4$ photoanode has a narrower bandgap of 2.4 eV versus RHE, which contributes to a high, theoretical solar-to-hydrogen conversion efficiency of 9.2% (Gan et al., 2014; Park et al., 2013). This remarkable efficiency has drawn tremendous research interest, yet its vulnerability to photocorrosion has been its weakness. $BiVO_4$ suffers from chemical instability in both acidic and alkaline conditions. Besides, its degradation is notably promoted by applied bias and light illumination when used as a photoanode in PEC (Lichterman et al., 2013; McDowell et al., 2014). Researchers have examined mainly three strategies to protect $BiVO_4$ electrodes against photocorrosion:

(a) Adopt an external passivation layer on the photoanode to avoid direct contact with the electrolyte (Fan et al., 1983; Hu et al., 2014; McDowell et al., 2014),

(b) Use co-catalysts to alter the thermodynamic reduction/oxidation potential of photo-generated holes/electrons, to facilitate oxygen/hydrogen evolution reactions instead of detrimental side reactions (Kim and Choi, 2014; Seabold and Choi, 2012; Zhong and Gamelin, 2009),

(c) Manipulate the electrolyte composition to retard dissolution. For example, when the electrolyte is saturated with V ions, dissolution of $BiVO_4$ photoanode is suppressed (Lee and Choi, 2017).

[1]School of Materials Science and Engineering, Nanyang Technological University, 50 Nanyang Avenue, Singapore 639798, Singapore

[2]Singapore-Berkeley Research Initiative for Sustainable Energy (SinBeRISE) CREATE Tower, 1 Create Way, #11-00, Singapore 138602, Singapore

[3]Institute of Materials Research and Engineering, 2 Fusionopolis Way, Singapore 138634, Singapore

[4]These authors contributed equally

[5]Lead Contact

*Correspondence: ASZChen@ntu.edu.sg (Z.C.), assritharan@ntu.edu.sg (T.S.)

https://doi.org/10.1016/j.isci.2019.08.037

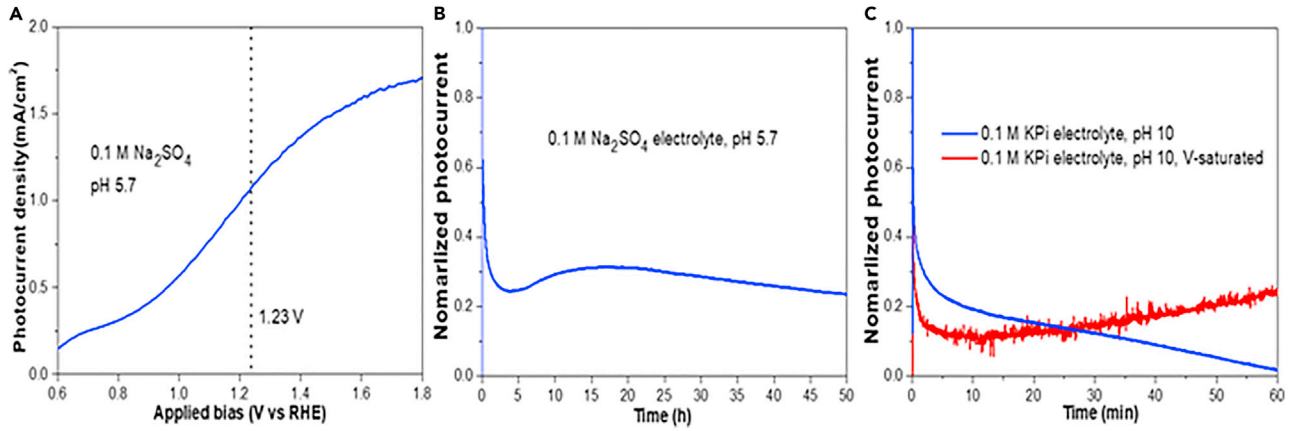

Figure 1. Performance and Stability of Mo-$BiVO_4$ Photoanode

(A) LSV curve of the Mo-$BiVO_4$ photoanode test under AM 1.5 G solar illumination and 1.23 V versus RHE bias, in 0.1 M Na_2SO_4 electrolyte (*pH* = 5.7). Dark current has already been netted from the photocurrent.

(B) Chronoamperometry of the test in (A) for continuous 50-h run.

(C) Chronoamperometry of Mo-$BiVO_4$ photoanode under AM 1.5 G solar illumination and 1.23 V versus RHE bias in 0.1 M KPi solution (*pH* = 10), with and without dissolved V_2O_5 species.

Considerable experimental effort has been devoted to the enhancement of stability via the three strategies, but the effort expended in understanding the degradation mechanism is limited. Several studies have fragmentally indicated the anodic photo-degradation propensity of the V ion in $BiVO_4$ (Ding et al., 2013; Lee and Choi, 2017; McDowell et al., 2014), which probably prompted Choi et al. to saturate the electrolyte with V ions to retard its degradation (Lee and Choi, 2017). Although, this approach reduced photo-degradation, it did not throw any light on the degradation mechanism. A recent study by Toma et al. did confirm the dissolution of V from $BiVO_4$, but it concluded that the rates of dissolution of both Bi and V would eventually become stoichiometric upon extensive corrosion (Toma et al., 2016). In this paper we propose a variation to this mechanism of degradation by in-depth mechanistic and theoretical studies that will contribute to the fundamental understanding. $BiVO_4$ has emerged as a versatile platform for understanding the photoelectrochemical behavior of transition metal oxide semiconductors (Sharp et al., 2017), where the observed material behavior could potentially be applied to similar types of materials.

RESULTS

$BiVO_4$ is usually used after doping with a higher valence metal ion (than V), such as Mo or W, to improve its electron conduction and charge separation (Zhao et al., 2018a, 2018b). In this work, we adopted n-type doping by 3 at% Mo, which enhances the photocurrent density (Luo et al., 2011). A 0.1 M Na_2SO_4 aqueous solution at *pH* = 5.7 was used as the electrolyte unless stated otherwise. The absorbance, reflectance, and transmittance data of the anode are in Figure S1. Performance of the photoanode was evaluated using linear scanning voltammetry (LSV) and chronoamperometry. Typical results obtained in a trial (Figure 1A) show an onset potential of ~0.6 *V* versus RHE and a photocurrent density of ~1.0 mA cm^{-2} at 1.23 V versus RHE (corresponding dark current is shown in Figure S2). Figure 1B shows the decline of the photocurrent (at 1.23 V versus RHE) normalized to the initial value with time, for 50 h of continuous PEC testing. The photocurrent decreased sharply to about 25% of the initial value in 4 h followed by a gradual decrease till the end of the test. This transition from short-term instability, in the time range 0–4 h, to long-term stability will be discussed later.

Trials were done in 0.1 M KPi electrolyte at *pH* = 10 saturated with V^{5+} ions, and without these ions, to assess the effect of pre-existing V ions on the degradation of the Mo-$BiVO_4$ photoanode. Saturation with V^{5+} ions was achieved by dissolving 0.1 M V_2O_5 powder in the electrolyte. A different electrolyte and *pH* became necessary to dissolve adequate V_2O_5 to saturate the solution with V^{5+}. Figure 1C shows that photocurrent in the V^{5+} saturated electrolyte became stable in 10 min, whereas that in the V-free electrolyte decreased continuously and eventually reached zero. Therefore, saturating the electrolyte with V^{5+} ions enhances the stability of Mo-$BiVO_4$ photoanode.

Light Illumination	Applied Bias (V versus RHE)	Duration (h)	Dissolution Rate on Bi Basis (nm h^{-1})	Dissolution Rate on V Basis (nm h^{-1})	Dissolution Rate on Mo Basis (nm h^{-1})	Bi:V	Affected Thickness (nm)
Dark	E_{OC}	99	2.4×10^{-6}	0.19	0.17	1:78,750	18.7
Dark	1.23	4	4.0×10^{-3}	2.78	0.91	1:695	11.1
Light	E_{OC}	4	6.5×10^{-4}	1.01	4.48	1:1,554	4.0
Light	1.23	4	0.19	4.56	4.64	1:24	18.2
Light	1.23	50	3.1×10^{-5}	0.45	1.20	1:14,407	22.5

Table 1. Dissolution Parameters Computed from ICP-MS Results of the Electrolyte after Photolysis under Different Conditions in 0.1 M Na_2SO_4 at *pH* = 5.7

See also Tables S1–S3. The affected thickness was calculated based on V dissolution rate. The calculation of dissolution rates and affected thicknesses are explained in Supplemental Information. The open circuit voltage EOC is shown in Figure S3 for both dark and light conditions.

After running the photoanode samples for different times under dark and illuminated conditions, concentrations of Bi, V, and Mo ions in the electrolyte were measured using an Inductively Coupled Plasma–Mass Spectrometer (ICP-MS). The applied bias, illumination, and temperature were controlled well so that they were not variable parameters. From the measured concentrations (see Table S1), average anode dissolution rates were calculated assuming spatially uniform dissolution over the entire photoelectrode (see Supplemental Information for calculation details). This gives different values when calculated for the concentrations of each of the elements Bi, V, and Mo. The initial thickness of the Mo-$BiVO_4$ film was 100 nm, which was reported previously (Yao et al., 2018). Tracking the dissolution rate through dissolved Mo could be inaccurate because some Mo could have deposited on the surface of $BiVO_4$ anode as MoO_3 during the anode synthesis (Luo et al., 2012). Yet, Mo could be used to calibrate V since it substitutes for V in the $BiVO_4$ crystal. The dissolution rates of Mo and V were consistent throughout, indicating the validity of these ICP-MS measurements.

Table 1 shows the uniform dissolution rates calculated from elemental concentrations, and the prevailing Bi:V atomic ratio in the electrolyte after some tests. It is striking that the Bi:V atomic ratio deviates significantly from the stoichiometric ratio 1:1 present in the $BiVO_4$ anode. There is excessive V (and Mo) compared with Bi in the electrolyte. The purely chemical dissolution rates are given by the dark and open circuit (E_{OC}) conditions, whereas the "PEC" condition indicates the photo-corrosion rates under both applied bias (1.23 V. versus RHE) and illumination. The chemical dissolution rates of V and Mo are higher than that of Bi by several orders of magnitude. The corrosion rates of all elements increase when either illumination or bias is applied, yet the Bi dissolution is always lower by a significant margin. Hence, V and Mo are more susceptible to dissolution under all conditions tested here. Table 1 shows the average thickness affected in the photoanode calculated using the rates of V dissolution. Interestingly, the affected thickness for three (first, fourth, and fifth) samples are very similar, even though their testing conditions are very different implying that the degradation has met strong resistance after an initial transient affecting a certain thickness. Such a resistance must have developed internally within the photoanode itself. This is supported by the chronoamperometry curve in Figure 1B, which shows that the photocurrent subsides to a steady value after a sharp reduction in the first 4 h.

For comparison, another set of photolysis trials was done using 0.1 M Na_2SO_4 electrolyte at *pH* = 7.0. The results are shown in Table S2. Decrease in the degradation rates is evident compared with *pH* = 5.7 probably due to relieved corrosion under the neutral condition. The calculated affected thicknesses for 4 h PEC and 90 h soaking conditions are similar indicating the development of self-resistance as for the case with *pH* = 5.7. The corresponding data for corrosion experiments conducted in *pH* = 8.3 electrolyte is shown in Tables S1 and S3. It must be noted that Toma et al. also examined the degradation of $BiVO_4$ in varied *pH* solutions. They too found the dissolution of V to be much faster than Bi in some *pH* electrolytes (Toma et al., 2016).

These results show that the degradation of Mo-$BiVO_4$ in 0.1 M Na_2SO_4 at *pH* = 5.7 and 7.0 is due to the preferential dissolution of V (and Mo) compared with Bi. Then, one needs to determine the destiny of the

Sample Condition	Bi (at.%)	V (at.%)	Mo (at.%)
Pristine	48.5	48.5	3.1
After 4 h degradation	58.7	38.2	3.1
After 50 h degradation	63.9	31.6	4.5

Table 2. XPS Quantitative Analysis of the Surface Composition of Different Photoanode Samples after Test Runs in 0.1 M Na_2SO_4 Electrolyte at *pH* = 5.7

Bi atoms released from the $BiVO_4$ crystals in the anode film as it degrades. Precipitation of solids was not detected in the electrolyte. This implies that Bi probably remains on the anode. Therefore, we scrutinized the anodes after the test runs by X-Ray Photoelectron Spectroscopy (XPS) for possible changes in its chemical composition. A summary of the calculated XPS surface chemical compositions is given in Table 2. The stoichiometric ratio of Bi:V = 1:1 was confirmed in pristine Mo-$BiVO_4$ to validate the XPS technique. After 4 h of PEC testing in *pH* = 5.7 electrolyte, the Bi:V ratio increased to approximately 1.5:1.0; after 50 h it increased to about 2:1. These results compliment the ICP-MS results, which showed negligible levels of Bi in the electrolyte, and confirm our hypothesis that Bi remains on the anode as it degrades. We attribute this Bi enrichment on the anode surface to the observed resistance to degradation, which amounts to self-passivation. Equation 1 shows a possible self-passivation reaction, where the solid Bi_2O_3 product could shield the surface of the $BiVO_4$ and protect it from further corrosion.

$$2\ BiVO_4 \leftrightarrow Bi_2O_3\ (s) + V_2O_5\ (soluble) \qquad \text{(Equation 1)}$$

This reaction, noted as R1, could be enabled by specific conditions, which will be clarified later in a theoretical discussion. Figure 2 shows the relevant high-resolution XPS spectra of Bi, V, and Mo. Shifts in the Bi 4f peaks evident in Figure 2A after degradation indicate that the product of degradation has a slightly lower binding energy (BE), signifying the formation of different Bi compounds on the surface, which probably constitutes the solid passivation layer. The BE of the Bi $4f_{7/2}$ and Bi $4f_{5/2}$ peaks in pristine Mo-$BiVO_4$ was measured to be 159.1 and 164.4 eV, respectively, consistent with a previous report (Liu et al., 2017). After long-term photodegradation, these peaks shifted to 158.9 and 164.2 eV, respectively. Figure 2B shows a shoulder around 531–534 eV in O 1s peak in the pristine Mo-$BiVO_4$, which is diminished after degradation. This was observed by previous workers also and was attributed to BE = 531.5 eV of the adsorbed O-H species on the surface of the as-fabricated anode (Qin et al., 2014; Zhang et al., 2014). The changes evident in the Mo spectrum of Figure 2C could be attributed to the dissolution of some MoO_3 that might have formed on the surface of Mo-$BiVO_4$ anode during the anode fabrication (solubility of MoO_3 is 0.490 g/100 mL at 28°C) (Liu et al., 2017).

Results of Electrochemical Impedance Spectroscopy (EIS) on the photoanode before and after photolysis are shown in Figure 2D. The diameter of the semicircle increased significantly after degradation, signifying an increase in the interfacial charge transfer resistance (R_{ct}) in the photoelectrode. Since all testing conditions remained unchanged, this increase of R_{ct} is likely due to a passivation layer, such as B_2O_3, which could increase the barrier for hole transport to the electrolyte at interface due to its energetically deeper valence band (Myung et al., 2011).

Figure 1B shows that 75% of the initial photocurrent was lost in the first 4 h, but the thickness affected, calculated using V concentration, is only 20% of that affected in 50 h. Therefore, we could attribute the loss of photocurrent in the first 4 h to charge transport retardation caused by the formation of the passivation layer rather than to rapid dissolution of $BiVO_4$.

Figure 3 shows the scanning electron micrographs of the photoanode before and after photolysis. Its porous nanostructure is evident. The surface before photolysis is relatively smooth, whereas after photolysis for 50 h (Figure 3B), it is degraded and rougher. However, its characteristic nanoporous structure is preserved. The roughness increase is probably caused by non-uniform degradation because of protection at specific locations from passivation. Therefore, microscopically, the photodegradation is not uniform across the illuminated area.

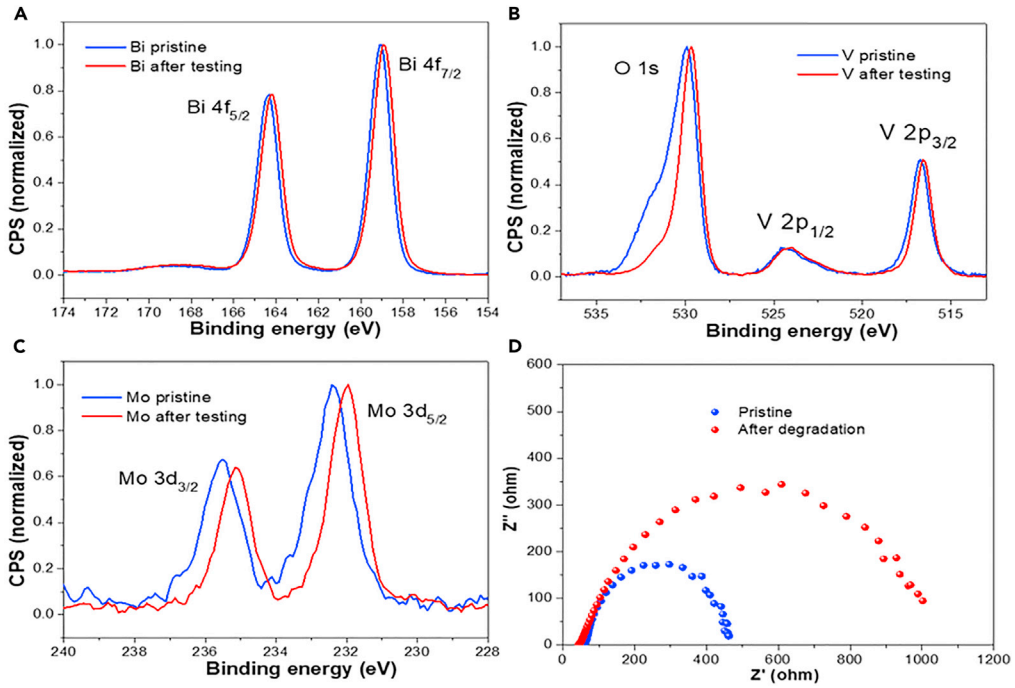

Figure 2. Characterization of Pristine Mo-$BiVO_4$ Photoanode and after Photolysis for 50 h in 0.1 M Na_2SO_4 Electrolyte at *pH* = 5.7

(A–C) High-resolution XPS spectra of Bi, V and O, and Mo.

(D) Nyquist plots.

With these determinative proofs, we could confirm the advent of a self-passivation mechanism in the photodegradation of Mo-$BiVO_4$ photoanode. Next, we employ computational modeling to validate the mechanism as well as to predict degradation products by theoretical means. First, we model the dark condition. The thermodynamic stability of pure Mo-$BiVO_4$ was simulated via a Pourbaix diagram established by Toma et al., which allows prediction of thermodynamic equilibrium and decomposition products (Hu et al., 2018; Persson et al., 2012; Pourbaix, 1966; Toma et al., 2016).

Figure 4A shows that Mo-$BiVO_4$ is thermodynamically stable only in relatively neutral electrolyte and at low external voltages. It would degrade in acidic or basic conditions, or when the voltage approaches the oxygen evolution potential. In comparison with the modeling results on pure $BiVO_4$, Mo-doping did not cause any material differences in its decomposition manner.

Simulation reveals two thermodynamically possible scenarios for degradation.

(a) A decomposition-based process: The solids Bi_4O_7 (B, O, P), Bi_2O_3 (D1, E1, I1, J1), and soluble ionic species VO_4^{3-}, HVO_4^{2-}, VO_3^- could form during degradation.

(b) An ion-exchange process: Another major region surrounding the stability region of Mo-$BiVO_4$ in the diagram involves the cation BiO^+, which would form solids with anions such as Cl^-, SO_4^{2-} (Bassett, 1965).

The Pourbaix diagram is based on thermodynamics only, whereas the actual mechanism will be influenced by kinetics and environmental factors also.

Then, we take illumination into account where photo-generated holes/electrons could participate in the self-oxidation/-reduction of $BiVO_4$ in addition to water splitting. Below we list all plausible oxidation/reduction reactions (R2–R17) to the best of our knowledge:

$$8\ BiVO_4 + O_2 + 4\ H_2O \leftrightarrow 2\ Bi_4O_7 + 8\ VO_3^- + 8\ H^+ \qquad \text{(Equation 2)}$$

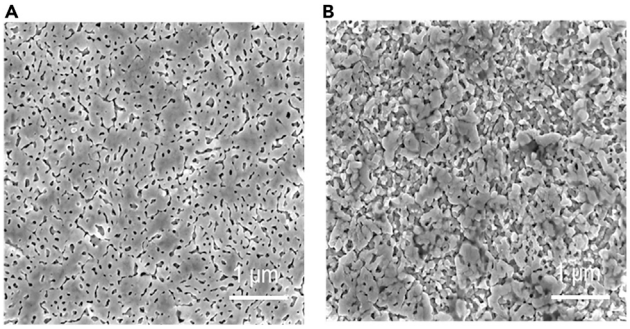

Figure 3. Scanning electron microscopy Images of the Mo-$BiVO_4$ Photoanode

(A) Pristine sample.

(B) Sample after photolysis for 50 h in 0.1 M Na_2SO_4 electrolyte at *pH* = 5.7.

See also Figure S4.

$$8\ BiVO_4 + O_2 + 12\ H_2O \leftrightarrow 2\ Bi_4O_7 + 8\ VO_4^{3-} + 24\ H^+ \quad \text{(Equation 3)}$$

$$4\ BiVO_4 + 7\ H_2O \leftrightarrow Bi_4O_7 + 4\ VO_4^{3-} + 12\ H^+ + H_2 \quad \text{(Equation 4)}$$

$$4\ BiVO_4 + 12\ H^+ \leftrightarrow 4\ Bi^{3+} + 2\ V_2O_5 + 6\ H_2 + 3\ O_2 \quad \text{(Equation 5)}$$

$$2\ BiVO_4 + 12\ H^+ \leftrightarrow 2\ Bi^{3+} + 2\ VOCl_3 + 6\ H_2 + 3\ O_2 \quad \text{(Equation 6)}$$

$$2\ BiVO_4 + H_2O \leftrightarrow 2\ BiVO_5 + H_2 \quad \text{(Equation 7)}$$

$$8\ BiVO_4 + H_2O \leftrightarrow 2\ Bi_4O_7 + 4\ V_2O_5 + H_2 \quad \text{(Equation 8)}$$

$$2\ BiVO_4 + O_2 \leftrightarrow 2\ BiVO_5 \quad \text{(Equation 9)}$$

$$8\ BiVO_4 + O_2 \leftrightarrow 2\ Bi_4O_7 + 4\ V_2O_5 \quad \text{(Equation 10)}$$

$$4\ BiVO_4 + 2\ H_2O + 4\ Cl^- \leftrightarrow 4\ VO_2 + 4\ BiOCl + 4\ OH^- + O_2 \quad \text{(Equation 11)}$$

$$2\ BiVO_4 + 2\ H^+ + 2\ Cl^- + H_2 \leftrightarrow 2\ VO_2 + 2\ BiOCl + 2\ H_2O \quad \text{(Equation 12)}$$

$$6\ BiVO_4 + 6\ Cl^- + 5\ H_2 \leftrightarrow 2\ H_2O + 2\ V_3O_5 + 6\ BiOCl + 6\ OH^- \quad \text{(Equation 13)}$$

$$2\ BiVO_4 + 3\ H_2 \leftrightarrow 2\ Bi + V_2O_5 + 3\ H_2O \quad \text{(Equation 14)}$$

$$2\ BiVO_4 + H_2 \leftrightarrow Bi_2O_3 + 2\ VO_2 + H_2O \quad \text{(Equation 15)}$$

$$2\ BiVO_4 + 5\ H_2 \leftrightarrow Bi_2O_3 + 2\ V + 5\ H_2O \quad \text{(Equation 16)}$$

$$BiVO_4 + 4\ H_2 \leftrightarrow Bi + 2\ V + 4\ H_2O \quad \text{(Equation 17)}$$

R2–R10 are oxidation reactions and R11–R17 are reduction reactions. Their propensity to occur could be assessed by their Gibbs free energy change.

Theoretically, thermodynamic oxidation and reduction potentials (ϕ^{ox} or ϕ^{re}) are indicative of the tendency for photo-corrosion of a semiconductor (Chen and Wang, 2012; Hu et al., 2018). Its resistance to photo-

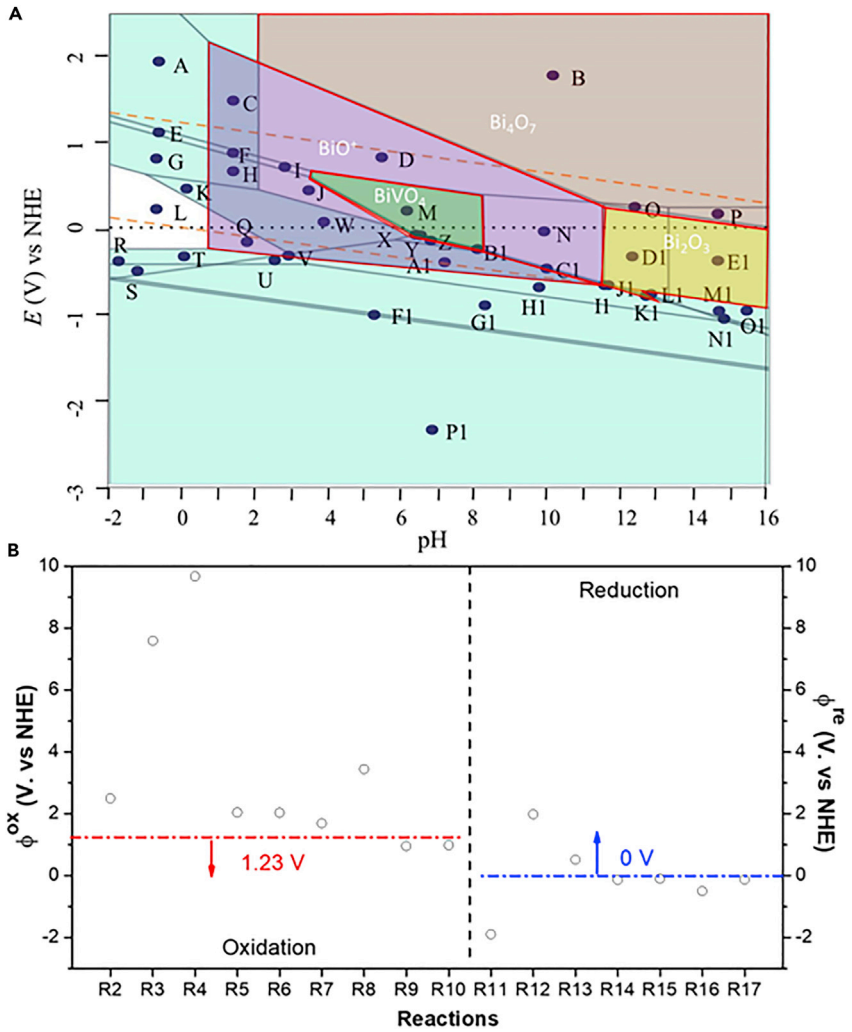

Figure 4. Thermodynamic Modeling Results

(A) The Pourbaix diagram of 50%–48%–2% Bi–V–Mo system in aqueous solution, assuming Bi, V, and Mo ion concentration at 10^{-8} mol kg^{-1}. Regions are labeled for stable phase(s) of: A – $MoO_3(s) + Bi^{3+} + VO_4^-$; B – $Bi_4O_7(s) + VO_4^- + MoO_4^{2-}$; C – $MoO_3(s) + BiO^+ + VO_4^-$; D – $BiO^+ + VO_4^- + MoO_4^{2-}$; E – $MoO_3(s) + Bi^{3+} + VO_2^+$; F – $MoO_3(s) + BiO^+ + VO_2^+$; G – $MoO_3(s) + Bi^{3+} + VO_2^+$; H – $MoO_3(s) + BiO^+ + VO_2^+$; I – $BiO^+ + VO_2^+ + MoO_4^{2-}$; J – $BiO^+ + VO_2^+ + MoO_4^{2-}$; K – $MoO_2(s) + Bi^{3+} + VO_2^+$; L – $Bi^{3+} + VO_2^+ + Mo^{3+}$; M – $BiVO_4(s) + BiO^+ + MoO_4^{2-}$; N – $BiO^+ + HVO_4^{2-} + MoO_4^{2-}$; O – $Bi_4O_7(s) + HVO_4^{2-} + MoO_4^{2-}$; P – $Bi_4O_7(s) + VO_4^{3-} + MoO_4^{2-}$; Q – $BiO^+ + VO_2^+ + Mo^{3+}$; R – $V_3Mo(s) + Bi(s) + VO_2^+$; S – $Mo(s) + Bi(s) + VO_2^+$; T – $Bi(s) + VO_2^+ + Mo^{3+}$; U – $Bi(s) + V_2O_3(s) + Mo^{3+}$; V – $BiO^+ + V_2O_3(s) + Mo^{3+}$; W – $MoO_2(s) + BiO^+ + VO_2^+$; X – $MoO_2(s) + VO_2(s) + BiO^+$; Y – $MoO_2(s) + BiVO_4(s) + BiO^+$; Z – $MoO_2(s) + V_3O_5(s) + BiO^+$; A1 – $MoO_2(s) + V_2O_3(s) + BiO^+$; B1 – $MoO_4^{2-} + V_3O_5(s) + BiO^+$; C1 – $MoO_4^{2-} + V_2O_3(s) + BiO^+$; D1 – $Bi_2O_3(s) + MoO_4^{2-} + HVO_4^{2-}$; E1 – $Bi_2O_3(s) + MoO_4^{2-} + VO_4^{3-}$; F1 – $V_3Mo(s) + Bi(s) + V_2O_3(s)$; G1 – $Mo(s) + Bi(s) + V_2O_3(s)$; H1 – $MoO_2(s) + Bi(s) + V_2O_3(s)$; I1 – $MoO_2(s) + Bi_2O_3(s) + V_2O_3(s)$; J1 – $Bi_2O_3(s) + V_2O_3(s) + MoO_4^{2-}$; K1 – $Bi(s) + V_2O_3(s) + MoO_4^{2-}$; L1 – $Bi(s) + HVO_4^{2-} + MoO_4^{2-}$; M1 – $Bi(s) + VO_4^{3-} + MoO_4^{2-}$; N1 – $Bi(s) + MoO_2 + VO_4^{3-}$; O1 – $Bi(s) + Mo(s) + VO_4^{3-}$; P1 – $V(s) + V_3Mo(s) + Bi(s)$.

(B) The calculated ϕ^{ox} and ϕ^{re} for the possible degradation processes of $BiVO_4$ with photo-generated electrons and holes.

corrosion largely depends on the alignment of its ϕ^{ox} relative to $\phi(O_2/H_2O)$ for the photoanode and ϕ^{re} relative to $\phi(H^+/H_2)$ for the photocathode. Corrosion is thermodynamically favorable when ϕ^{ox} is smaller than $\phi(O_2/H_2O)$ or when ϕ^{re} is higher than $\phi(H^+/H_2)$ where the values are defined by the listed reactions R1 to R17 and calculated based on changes in Gibbs free energy given by Equations 18 and 19,

$$\phi^{re} - \phi(H^+/H2) = -[\sum G(products) - \sum G(reactants)]/nEF \qquad \text{(Equation 18)}$$

$$\phi^{ox} - \phi(H^+/H2) = [\sum G(prodcuts) - \sum G(reactants)]/nEF \quad \text{(Equation 19)}$$

where, n is the number of photo-generated holes/electrons, *G(products)* and *G(reactants)* stand for the Gibbs free energy of products and reactants, respectively, which are available in the literature (Jain et al., 2013; Lide, 2003–2004).

As shown in Figure 4B, the calculated ϕ^{ox} values for R9 and R10 are lower than $\phi(O_2/H_2O)$, and ϕ^{re} for R12, R13 are higher than $\phi(H^+/H_2)$, which makes these four degradation reactions thermodynamically favorable. Therefore, $BiVO_4$ would be susceptible to both oxidation of holes and reduction of electrons in aqueous solution under illumination. Among them, R10 appears to be the most probable reaction and is also consistent with our experimental observation as V_2O_5 could get dissolved in the electrolyte, whereas Bi oxide solid could be retained on the photoanode. Since we applied a bias of 1.23 V versus RHE to mimic the condition of electrochemical solar water splitting, the environment around Mo-$BiVO_4$ photoanode should be oxidative. The R10 reaction itself occurs in strongly oxidative conditions, which could emanate from a high voltage bias, accumulation of photo-generated holes at the surface, or abundance of reactive oxygen species (OH^- and O^-) during the water splitting process. The stability of $BiVO_4$ is determined by the competitive reactions between the self-oxidation/reduction and water splitting. By introducing co-catalysts, the water-splitting potential could be enhanced in comparison with self-oxidation/reduction reactions, thereby improving the long-term stability of the semiconductor.

DISCUSSION

Accumulation of Bi on the photoanode, accompanied by development of self-resistance to further corrosion was proven by ICP-MS, XPS, chronoamperometry, and EIS investigations in this study. Hence, a passivation layer appears to form by degradation of the $BiVO_4$ on the surface of the photoanode under our photolysis conditions. This self-passivation mechanism is supported by thermodynamic computations, which predict two categories of degradation products, namely, bismuth oxides (Bi_2O_3, Bi_4O_7) and $(BiO)_2SO_4$. Next, we scrutinize our samples for these predicted degradation products.

XPS was used to examine the possibility of $(BiO)_2SO_4$ formation. Normally, the BE of S 2p peak in sulfates is in the region 168–172 eV (Wagner and Mullenberg, 1979; Wahlqvist and Shchukarev, 2007). Since no peaks were detected in this BE range in the degraded anode samples, as evident in Figures 2A and S4, the possibility of $(BiO)_2SO_4$ formation is not substantiated. This makes bismuth oxides as the possible degradation products.

Subsequent characterizations by XPS, UV-vis, and Fourier-transform infrared spectroscopy (FTIR) provided less definitive results to conclusively identify the degradation products but gave some important evidence that are included in Supplemental Information. To be specific, the Bi 4f peaks in commercial Bi_2O_3 are shifted to lower BE (158.5 and 163.8 eV from Figure S7) compared with those in $BiVO_4$ (159.1 and 164.4 eV), which concurs with Bi peak shifts observed in the photoanode samples after degradation (Figure 2A). From the UV-vis spectra (Figure S8), after degradation the photoanode showed increased absorbance in the range of 310–460 nm, which coincides with the main absorbance range of Bi_2O_3. Besides, we detected VO_4^{3-} by FTIR spectra (Figure S9) in the electrolyte after photolysis, which indicates the formation of bismuth oxides according to those degradation reactions discussed earlier. Combining these experimental results, we conclude that bismuth oxides are the most probable degradation products because their formation is not negated by investigations on the photoanode and the electrolyte. We would suggest Bi_2O_3 or Bi_4O_7 to be the major components of degradation products on the photoanode. Bi_4O_7 is more thermodynamically favorable in the strongly oxidative condition used for PEC photolysis.

In summary, we used Mo-doped $BiVO_4$ as a platform to elucidate the mechanism of degradation of $BiVO_4$ photoanode during photoelectrochemical water splitting in 0.1 M Na_2SO_4 electrolyte at $pH = 5.7$. The results gave strong evidence for the preferential dissolution of V (probably as VO_4^{3-}, HVO_4^{2-}, VO_3^-) during photolysis, in comparison with Bi. Besides, strong evidence obtained indicates that Bi remains on the anode surface as a solid remnant product, likely as Bi_2O_3 or Bi_4O_7. Complementary thermodynamic modeling and analyses of possible reactions under the prevailing conditions gave this degradation mechanism a sound theoretical backup. $BiVO_4$ undergoes even a purely chemical dissolution in the said electrolyte, but it gets accelerated by illumination and external bias application during photolysis. Enrichment of

the surface by the Bi-containing remnant product, a consequence of degradation, appears to passivate the photoanode and protect it from extensive degradation over long periods of photolysis. This unforeseen benefit, however, comes at the expense of charge-transport kinetics, which results in a decrease in photocurrent density. Evidence to conclusively identify the passivation compound was not found, but experimental and theoretical verifications support the possibility of the oxides Bi_2O_3 and/or Bi_4O_7 as the major constituents of the passivation layer.

Limitations of the Study

Although this study advances the current understanding of the degradation mechanism of $BiVO_4$ in PEC photolysis, the investigations were in a specific electrolyte only. The degradation of $BiVO_4$ in other common electrolytes remains to be elucidated. The degradation product could not be conclusively identified experimentally, although thermodynamic modeling pointed to either Bi_2O_3 or Bi_4O_7. A kinetic model needs to be developed to describe the degradation process accurately once the degradation product is confirmed.

METHODS

All methods can be found in the accompanying Transparent Methods supplemental file.

SUPPLEMENTAL INFORMATION

Supplemental Information can be found online at https://doi.org/10.1016/j.isci.2019.08.037.

ACKNOWLEDGMENTS

Authors would like to thank National Research Foundation, Singapore for funding the CREATE Program Singapore-Berkeley Research Initiative for Sustainable Energy (SinBeRISE) under which this project was done.

AUTHOR CONTRIBUTIONS

Conceptualization and methodology, X.Y., Z.C., and T.S.; Investigation, X.Y. and X.Z.; Modeling, J.H.; Characterization, H.X., D.W., X.C., Z.Z.; Writing – Original Draft, X.Y.; Writing – Review & Editing, T.S.; Resources, Y.H.; Funding Acquisition, T.S.; Supervision, Z.C. and T.S.

DECLARATION OF INTERESTS

The authors declare no competing financial interest.

Received: January 13, 2019
Revised: July 15, 2019
Accepted: August 20, 2019
Published: September 27, 2019

REFERENCES

Barber, J. (2009). Photosynthetic energy conversion: natural and artificial. Chem. Soc. Rev. *38*, 185–196.

Bassett, J. (1965). Inorganic Chemistry: A Concise Text (Pergamon).

Blankenship, R.E., Tiede, D.M., Barber, J., Brudvig, G.W., Fleming, G., Ghirardi, M., Gunner, M.R., Junge, W., Kramer, D.M., Melis, A., et al. (2011). Comparing photosynthetic and photovoltaic efficiencies and recognizing the potential for improvement. Science *332*, 805–809.

Chen, S., and Wang, L.-W. (2012). Thermodynamic oxidation and reduction potentials of photocatalytic semiconductors in aqueous solution. Chem. Mater. *24*, 3659–3666.

Ding, C., Shi, J., Wang, D., Wang, Z., Wang, N., Liu, G., Xiong, F., and Li, C. (2013). Visible light driven overall water splitting using cocatalyst/$BiVO_4$ photoanode with minimized bias. Phys. Chem. Chem. Phys. *15*, 4589–4595.

Fan, F.-R.F., Keil, R.G., and Bard, A.J. (1983). Photooxidation of halides and water on n-silicon protected with silicide layers. J. Am. Chem. Soc. *105*, 220–224.

Fujishima, A., and Honda, K. (1972). Electrochemical photolysis of water at a semiconductor electrode. Nature *238*, 237–238.

Gan, J., Lu, X., and Tong, Y. (2014). Towards highly efficient photoanodes: boosting sunlight-driven semiconductor nanomaterials for water oxidation. Nanoscale *6*, 7142–7164.

Grätzel, M. (2001). Photoelectrochemical cells. Nature *414*, 338–344.

Gust, D., Moore, T.A., and Moore, A.L. (2009). Solar fuels via artificial photosynthesis. Acc. Chem. Res. *42*, 1890–1898.

Hu, J., Chen, W., Zhao, X., Su, H., and Chen, Z. (2018). Anisotropic electronic characteristics, adsorption, and stability of low-index $BiVO_4$ surfaces for photoelectrochemical applications. ACS Appl. Mater. Inter. *10*, 5475–5484.

Hu, S., Shaner, M.R., Beardslee, J.A., Lichterman, M., Brunschwig, B.S., and Lewis, N.S. (2014). Amorphous TiO_2 coatings stabilize Si, GaAs, and GaP photoanodes for efficient water oxidation. Science *344*, 1005–1009.

Jain, A.O., Ong, S.P., Hautier, G., Chen, W., Richards, W.D., Dacek, S., Cholia, S., Gunter, D., Skinner, D., Ceder, G., and Persson, K. (2013). A commentary: the materials project: a materials genome approach to accelerating materials innovation. APL Mater. *1*, 011002.

Kim, T.W., and Choi, K.S. (2014). Nanoporous $BiVO_4$ photoanodes with dual-layer oxygen evolution catalysts for solar water splitting. Science *343*, 990–994.

Lee, D.K., and Choi, K.-S. (2017). Enhancing long-term photostability of $BiVO_4$ photoanodes for solar water splitting by tuning electrolyte composition. Nat. Energy *3*, 53–60.

Lewis, N.S., and Nocera, D.G. (2006). Powering the planet: chemical challenges in solar energy utilization. Proc. Natl. Acad. Sci. U S A *103*, 15729–15735.

Li, Z., Luo, W., Zhang, M., Feng, J., and Zou, Z. (2013). Photoelectrochemical cells for solar hydrogen production: current state of promising photoelectrodes, methods to improve their properties, and outlook. Energy Environ Sci. *6*, 347–370.

Lichterman, M.F., Shaner, M.R., Handler, S.G., Brunschwig, B.S., Gray, H.B., Lewis, N.S., and Spurgeon, J.M. (2013). Enhanced stability and activity for water oxidation in alkaline media with bismuth vanadate photoelectrodes modified with cobalt oxide catalytic layer produced by atomic layer deposition. J. Phys. Chem. Lett. *4*, 4188–4191.

Lide, D.R. (2003—2004). CRC. Handbook of Chemistry and Physics, 84th Edition (CRC Press).

Liu, B., Yan, X., Yan, H., Yao, Y., Cai, Y., Wei, J., Chen, S., Xu, X., and Li, L. (2017). Preparation and characterization of Mo doped in $BiVO_4$ with enhanced photocatalytic properties. Materials *10*, 976.

Luo, W., Li, Z., Yu, T., and Zou, Z. (2012). Effects of surface electrochemical pretreatment on the photoelectrochemical performance of Mo-doped $BiVO_4$. J. Phys. Chem. C *116*, 5076–5081.

Luo, W., Yang, Z., Li, Z., Zhang, J., Liu, J., Zhao, Z., Wang, Z., Yan, S., Yu, T., and Zou, Z. (2011). Solar hydrogen generation from seawater with a modified $BiVO_4$ photoanode. Energy Environ Sci. *4*, 4046–4051.

Maeda, K., and Domen, K. (2010). Photocatalytic water splitting: recent progress and future challenges. J. Phys. Chem. Lett. *1*, 2655–2661.

McDowell, M.T., Lichterman, M.F., Spurgeon, J.M., Hu, S., Sharp, I.D., Brunschwig, B.S., and Lewis, N.S. (2014). Improved stability of polycrystalline bismuth vanadate photoanodes by use of dual-Layer thin TiO_2/Ni coatings. J. Phys. Chem. C *118*, 19618–19624.

Myung, N., Ham, S., Choi, S., Chae, Y., Kim, W.-G., Jeon, Y.J., Paeng, K.-J., Chanmanee, W., de Tacconi, N.R., and Rajeshwar, K. (2011). Tailoring interfaces for electrochemical synthesis of semiconductor films: $BiVO_4$, Bi_2O_3, or composites. J. Phys. Chem. C *115*, 7793–7800.

Park, Y., McDonald, K.J., and Choi, K.S. (2013). Progress in bismuth vanadate photoanodes for use in solar water oxidation. Chem. Soc. Rev. *42*, 2321–2337.

Persson, K.A., Waldwick, B., Lazic, P., and Ceder, G. (2012). Prediction of solid-aqueous equilibria: scheme to combine first-principles calculations of solids with experimental aqueous states. Phys. Rev. B *85*, 235438.

Pourbaix, M. (1966). Atlas of Electrochemical Equilibria in Aqueous Solutions (Pergamon Press).

Qin, D.D., Wang, T., Song, Y.M., and Tao, C.L. (2014). Reduced monoclinic $BiVO_4$ for improved photoelectrochemical oxidation of water under visible light. Dalton Trans. *43*, 7691–7694.

Seabold, J.A., and Choi, K.S. (2012). Efficient and stable photo-oxidation of water by a bismuth vanadate photoanode coupled with an iron oxyhydroxide oxygen evolution catalyst. J. Am. Chem. Soc. *134*, 2186–2192.

Sharp, I.D., Cooper, J.K., Toma, F.M., and Buonsanti, R. (2017). Bismuth vanadate as a platform for accelerating discovery and development of complex transition-metal oxide photoanodes. ACS Energy Lett *2*, 139–150.

Sivula, K., and van de Krol, R. (2016). Semiconducting materials for photoelectrochemical energy conversion. Nat. Rev. Mater. *1*, 15010.

Toma, F.M., Cooper, J.K., Kunzelmann, V., McDowell, M.T., Yu, J., Larson, D.M., Borys, N.J., Abelyan, C., Beeman, J.W., Yu, K.M., et al. (2016). Mechanistic insights into chemical and photochemical transformations of bismuth vanadate photoanodes. Nat. Commun. *7*, 12012.

Wagner, C.D., and Mullenberg, G.E. (1979). Handbook of X-Ray Photoelectron Spectroscopy: A Reference Book of Standard Data for Use in X-ray Photoelectron Spectroscopy (Perkin-Elmer Corp.).

Wahlqvist, M., and Shchukarev, A. (2007). XPS spectra and electronic structure of Group IA sulfates. J. Electron Spectrosc. Relat. Phenom. *156–158*, 310–314.

Walter, M.G., Warren, E.L., McKone, J.R., Boettcher, S.W., Mi, Q., Santori, E.A., and Lewis, N.S. (2010). Solar water splitting cells. Chem. Rev. *110*, 6446–6473.

Yao, X., Wang, D., Zhao, X., Ma, S., Bassi, P.S., Yang, G., Chen, W., Chen, Z., and Sritharan, T. (2018). Scale-up of $BiVO_4$ photoanode for water splitting in a photoelectrochemical cell: issues and challenges. Energy Technol. *6*, 100–109.

Zhang, Y., Guo, Y., Duan, H., Li, H., Sun, C., and Liu, H. (2014). Facile synthesis of V^{4+} self-doped, [010] oriented $BiVO_4$ nanorods with highly efficient visible light-induced photocatalytic activity. Phys. Chem. Chem. Phys. *16*, 24519–24526.

Zhao, X., Hu, J., Chen, S., and Chen, Z. (2018a). An investigation on the role of W doping in $BiVO_4$ photoanodes used for solar water splitting. Phys. Chem. Chem. Phys. *20*, 13637–13645.

Zhao, X., Hu, J., Yao, X., Chen, S., and Chen, Z. (2018b). Clarifying the roles of oxygen vacancy in W-doped $BiVO_4$ for solar water splitting. ACS Appl. Energy Mater. *1*, 3410–3419.

Zhong, D.K., and Gamelin, D.R. (2009). Photoelectrochemical water oxidation by cobalt catalyst ("Co-Pi")/r-Fe_2O_3 composite photoanodes: oxygen evolution and resolution of a kinetic bottleneck. J. Am. Chem. Soc. *132*, 4202–4207.

ISCI, Volume *19*

Supplemental Information

The Self-Passivation Mechanism in Degradation of $BiVO_4$ Photoanode

Xin Yao, Xin Zhao, Jun Hu, Huiqing Xie, Danping Wang, Xun Cao, Zheng Zhang, Yizhong Huang, Zhong Chen, and Thirumany Sritharan

SUPPLEMENTAL

Transparent Methods

Synthesis. Synthesis and detailed characterizations of the Mo-$BiVO_4$ photoanode can be found in our previous report (Yao et al., 2018). Briefly, we mixed $Bi(NO_3)_3 \cdot 5H_2O$ (Sigma-Aldrich, ≥ 98.0%, 0.2 mol L^{-1}) in glacial acetic acid (Sigma-Aldrich), vanadyl acetylacetonate (Sigma-Aldrich, 99.98% trace metals basis, 0.03 mol L^{-1}) in acetylacetone (Sigma-Aldrich, ≥ 99.0%) and molybdenyl acetylacetonate (Sigma-Aldrich, 0.01 mol L^{-1}) in acetylacetone with a 100 : 97 : 3 ratio of Bi : V : Mo, and then diluted the mixture by 3 times with acetylacetone. The diluted solution (60 μL) was evenly drop cast onto a 1 cm × 2 cm FTO glass (13.4 Ω $□^{-1}$, Latech, Singapore), which was placed on a 50°C hotplate. The solution would spread across the entire surface of FTO substrate evenly, driven by the surface tension between solvent and the FTO surface. No further action is required to spread the solution. After drop casting, the solution will gradually dry on the FTO glass formation $BiVO_4$ film. After complete drying, the FTO glass substrate with the dried precursor was transferred to the furnace for calcination at 470°C for 30 min, followed by air cooling to room temperature. This forms a relatively homogenous thin film coating. For electrochemical measurements, the edge of Mo-$BiVO_4$ coating was etched away by HCl, to leave a margin for electrical wire connection. The actual photoactive area ws 1.2 cm^2 or 1.3 cm^2 for water splitting.

Photoelectrochemical characterization. The electrochemical measurement was conducted on a PCI4/300™ potentiostat (with the PHE200™ software, Gammy Electronic Instruments, Inc.), in a three-electrode configuration. The FTO/Mo-$BiVO_4$ sample served as the working electrode, with a platinum foil as counter electrode and Ag/AgCl (4 M KCl) as reference electrode. The potential measured vs. the Ag/AgCl reference electrode can be converted to the potential vs. RHE by the following equation.

$$E\ (\text{vs. RHE}) = E(\text{vs. Ag/AgCl}) + E_{Ag/AgCl}(\text{reference}) + 0.0591 \times pH$$

$E_{Ag/AgCl}$(reference) = 0.1976 V vs. NHE at 25°C

The light source was a Xe lamp (300 W, HAL-320, Asahi Spectra Co., Ltd) equipped with AM 1.5G filter, and the light intensity irradiated at the center of working electrode was adjusted to 100 mW cm^{-2}. The light was always irradiated on the front side film. Linear sweep voltammetry was performed at a scan rate of 30 mV s^{-1}. During the photo-corrosion process, the Mo-$BiVO_4$ samples were fully immersed in the electrolyte without any mask. Different amounts of electrolyte were used for different durations of test to get conveniently detectable concentrations of ions; for the 50 h duration, 100 mL electrolyte was used. Water cooling was used to remove the heat generated by light illumination. We mainly used 0.1 M Na_2SO_4 (Aladin, 99.999% metal basis) solution at *pH* = 5.7 as the electrolyte. 0.1 M neutral (*pH* = 7) Na_2SO_4 electrolyte was also used as the control group, and its *pH* was manually tuned to 7 by dilute NaOH (Sigma-Aldrich, 99.99% metal basis) solution. The *pH* for neutral Na_2SO_4 will decrease over time since it's not a buffer solution. During the corrosion process, the *pH* value was constantly monitored by a *pH* meter (CyberScan series 600, Eutech Instruments) and adjusted accordingly. KPi electrolyte was prepared by dissolving KH_2PO_4 (Sigma-Aldrich, 99.99% trace metals basis) in distilled water, and its pH was adjusted by KOH (Sigma-Aldrich, 99.99% metal basis) pellets. The V-saturated electrolyte was prepared according to Choi's work (Lee and Choi, 2017). Alternating current impedance spectroscopy was tested within the frequency range 100,000 – 0.2 Hz, with applied bias of 1.23 V vs. RHE under light illumination.

Calculation of dissolution rates:

- We assume uniform degradation over the whole anode area starting from the surface. This helps us to compare degradation rates under different experimental conditions, and also gives us a quantitative estimate of the dissolved matter.
- Using the concentration of each element measured by ICP-MS in the electrolyte, we calculate the total number of moles of that particular element that is dissolved in the electrolyte (n_D).

- The number of moles of each element available in the initial $BiVO_4$ film (n_F) could be computed from the amount of precursor used for its synthesis. The initial thickness of the film (h_F =100 nm) was also measured.
- Now we can calculate the film thickness that needs to be dissolved (h_D) to attain the measured molar concentration in the electrolyte for each element, assuming uniform film dissolution, by using the following equation.

  $h_D = h_F \times (n_D / n_F)$
- Dividing h_D by the experiment duration (t) gives the dissolution rate for each element, as below:

  $R_D = h_D / t$
- Due to unequal measured concentration for each element in the electrolyte, the dissolved film thickness calculated for each element is different. In this work, we used the affected thickness of the film computed from V concentration as the true h_D as V has the highest concentration.

Materials characterization. ICP-MS was carried out on ELAN DRC II (Perkin Elmer) where the detection limit is at ppt level. The solution samples were first diluted to 10 or 100 times and then digested by 1% nitric acid prior to measurement. XPS was conducted on PHI Quantera SXM Scanning X-Ray Microprobe, with Al K_α incident X-rays. All the spectra were calibrated by shifting their C 1s core level position to 284.8 eV. Field emission SEM images were collected from JSM-7600F (JOEL) and FEI Nova Nanolab 600i (TSS microscopy). Grazing-angle XRD was performed on Shimadzu XRD-6000 (Shimadzu) by using Cu K_α radiation at 40 kV and 30 mA, and the incident angle was 1°. The UV-vis spectroscopy was obtained from LAMBDA 750 (Perkin Elmer), where the absorbance spectra of thin film samples were obtained by measuring the reflectance and transmittance spectra with an integrating sphere. FTIR was carried out on Frontier FTIR/NIR spectrometer (Perkin Elmer). Raman spectroscopy was conducted on Jobinyvon U1000 spectrometer (Horiba) with a 514 nm laser at room temperature.

Theoretical modelling. By referring to the work of Persson *et al*. (Persson et al., 2012), we used the hybrid calculated-experimental Pourbaix formalism approach to acquire the Pourbaix diagram implemented in Materials Project. The phase diagrams app47 from the Materials Project database was employed to establish the phase diagram for our Bi-V-Mo-O system. The phase diagram at 0 K and 0 atm could be derived by calculating the energy for all known products composed of the four elements. We used a database of Density Functional Theory calculations to acquire the reaction calculator's energies, and the Ab Initio Simulation Package (VASP) was used with the exchange-correlational function (Kresse, 1996). The Gibbs free energy for the reactants and products involved in our proposed reactions were available from the handbooks and journal publications.

Electrolyte	Light illumination	Bias (V vs. RHE)	Duration (h)	Volume (mL)*	Sample size (cm^2)	Bi (ppb)	V (ppb)	Mo (ppb)
0.1 M Na_2SO_4 *pH* 5.7	Dark	E_{OC}	99 h	5	2	0.05	924.58	49.25
	Dark	1.23	4 h	20	1.3	0.58	89.93	1.71
	Light	E_{OC}	4 h	20	1.3	0.09	32.70	8.40
	Light	1.23	4 h	20	1.3	26.89	147.50	8.70
	Light	1.23	50 h	100	1.2	0.01	33.04	5.18
0.1 M Na_2SO_4 *pH* 7	Dark	E_{OC}	96 h	5	2	0.4	458.13	59.23
	Dark	1.23	4 h	25	1.3	0.3	53.95	5.86
	Light	E_{OC}	4 h	25	1.3	0.08	38.74	6.70
	Light	1.23	4 h	25	1.3	1.26	58.05	6.40
0.1 M KPi *pH* 8.3	Dark	1.23	5 h	25	1.3	30.50	90.16	5.18
	Light	1.23	5 h	25	1.3	76.00	718.87	18.75

Table S1. Concentrations of Bi, V and Mo obtained by ICP-MS in three electrolytes, related to Table 1. Note the high concentration of Bi in 5 h of testing in the 0.1 M KPi electrolyte at *pH* = 8.3. *Volume of electrolyte used for the photolysis run

From 4 h to 50 h degradation, the Bi concentration has decreased, contrary to expectation, by about 4 orders of magnitude. This could be because of re-deposition of dissolved Bi back on the anode surface (probably in the form of bismuth oxide) as the solid oxide is thermodynamically favored under illumination and applied bias.

Light illumination	**Applied bias (V vs. RHE)**	**Duration (h)**	**Dissolution rate on Bi basis (nm/h)**	**Dissolution rate on V basis (nm/h)**	**Dissolution rate on Mo basis (nm/h)**	**Bi: V**	**Affected thickness (nm)**
Dark	E_{OC}	96	2.0×10^{-5}	0.096	0.21	1:483	9.2
Dark	1.23	4	2.7×10^{-3}	2.09	3.90	1:772	8.3
Light	E_{OC}	4	7.2×10^{-4}	1.50	4.47	1:208	6.0
Light	1.23	4	0.011	2.24	4.23	1:198	9.0

Table S2. ICP-MS results of the electrolyte after photolysis using Mo:$BiVO_4$ photoanodes under different conditions in 0.1 M Na_2SO_4 electrolyte at *pH* = 7.0, related to Table 1.

Light illumination	Applied bias (V vs. RHE)	Duration (h)	Dissolution rate on Bi basis	Dissolution rate on V basis	Dissolution rate on Mo basis	Bi: V	Affected thickness (nm)
Dark	1.23	5	0.22	2.79	2.67	1:12.7	14.0
Light	1.23	5	0.55	22.23	10	1:40.6	111.2

Table S3. ICP-MS results of the electrolyte after photolysis using Mo:$BiVO_4$ photoanodes in 0.1 M KPi solution at *pH* = 8.3, related to Table 1.

The ICP-MS data collected from 0.1 M KPi solution (*pH* = 8.3) also indicated much higher dissolution rate of V in comparison to Bi. It can be seen that at this *pH* value, the loss of V is quite radical. Toma et al also conducted ICP-MS analysis for 0.1 M KPi solution (*pH* = 6.8 and *pH* = 12.3) (Toma et al., 2016). They too found that the dissolution of V is much faster than Bi in both electrolytes which is in agreement with our results.

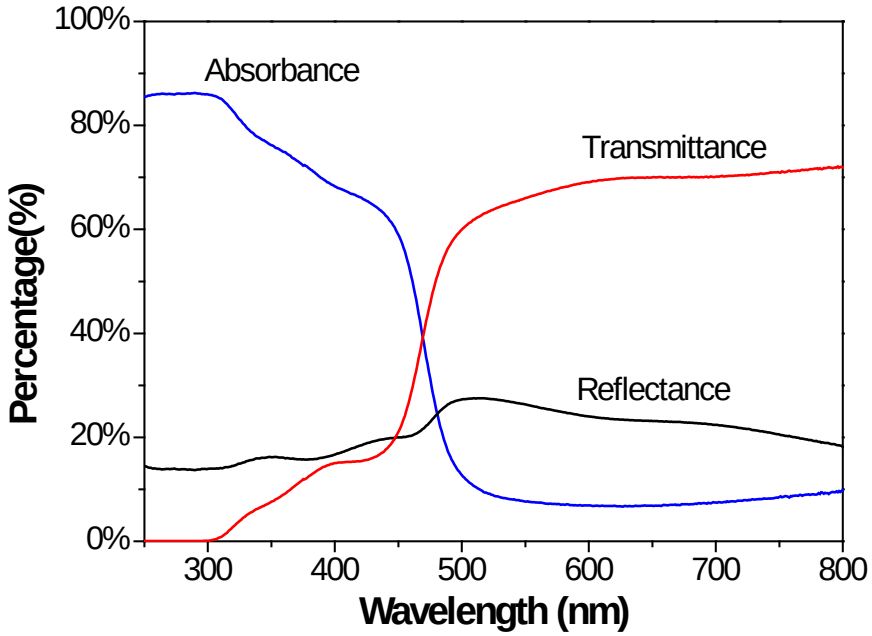

Figure S1. Absorbance, reflectance and transmittance of the Mo-$BiVO_4$ photoanode backed by FTO glass, related to Figure 1.

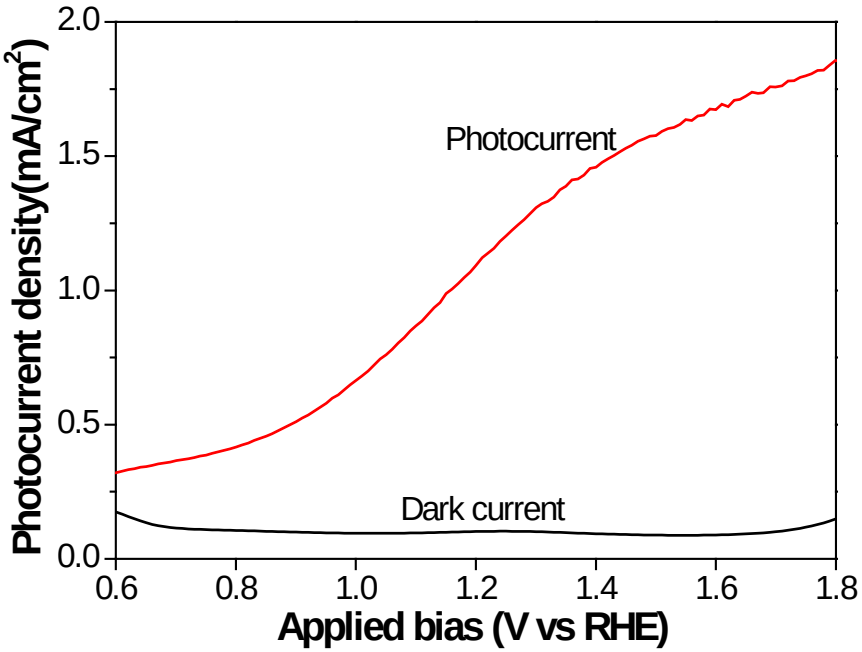

Figure S2. Photocurrent and dark current densities of 0.25 cm^2 Mo-$BiVO_4$ photoanode, related to Figure 1.

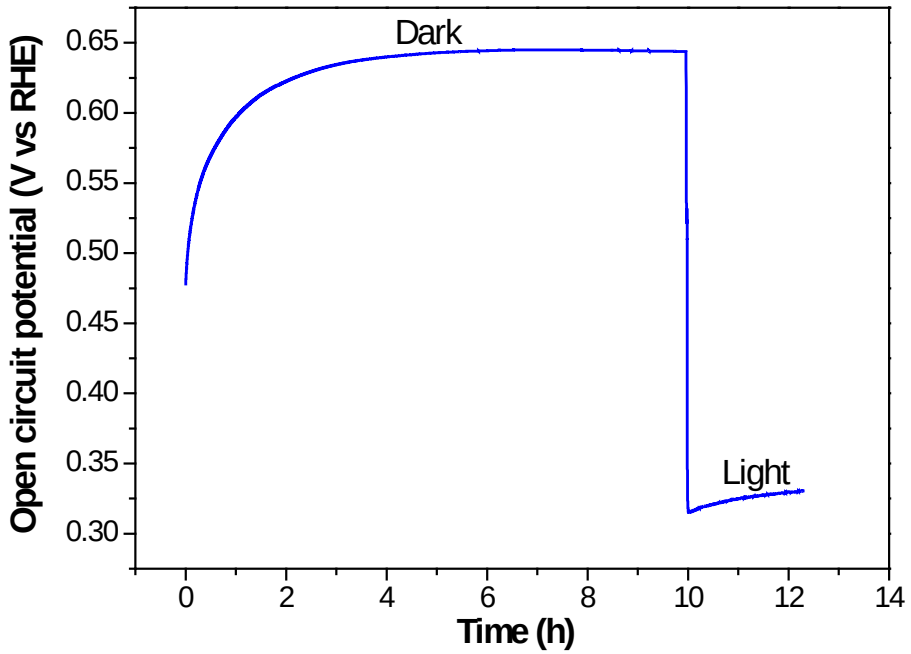

Figure S3. Open circuit potential of Mo-$BiVO_4$ in dark and illuminated conditions, related to Table 1.

The open circuit potential of Mo-$BiVO_4$ photoanode in PEC for the dark and illuminated conditions are 0.646 V and 0.331 V respectively.

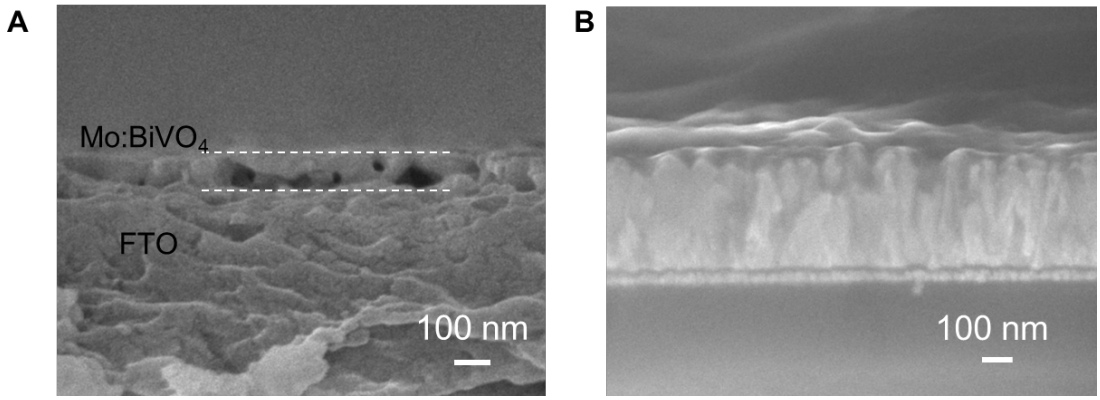

Figure S4. Cross-sectional SEM images of the Mo-BiV_4 thin film, related to Figure 3.

(A) Before photolysis. (B) After photolysis for 50 h.

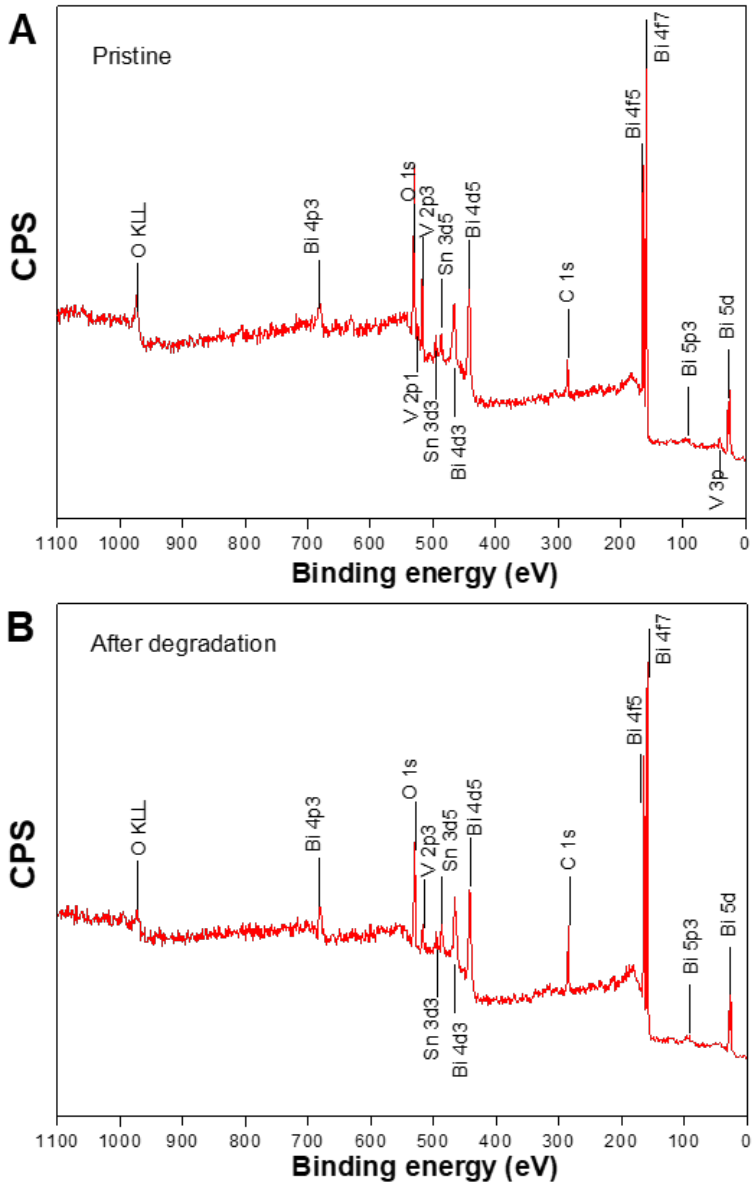

Figure S5. XPS spectrum for the Mo-BiV$_4$ photoanode, related to Figure 4.

(A) Before photolysis. (B) After photolysis for 50 h.

As shown in the XPS full spectrum of Figure S5, the V 2p$_{1/2}$ and V 3p peaks in the pristine Mo-BiV$_4$ photoanode were diminished after 50 h continuous photolysis, indicating the intensive loss of vanadium. Peaks of sulfur were not detected here.

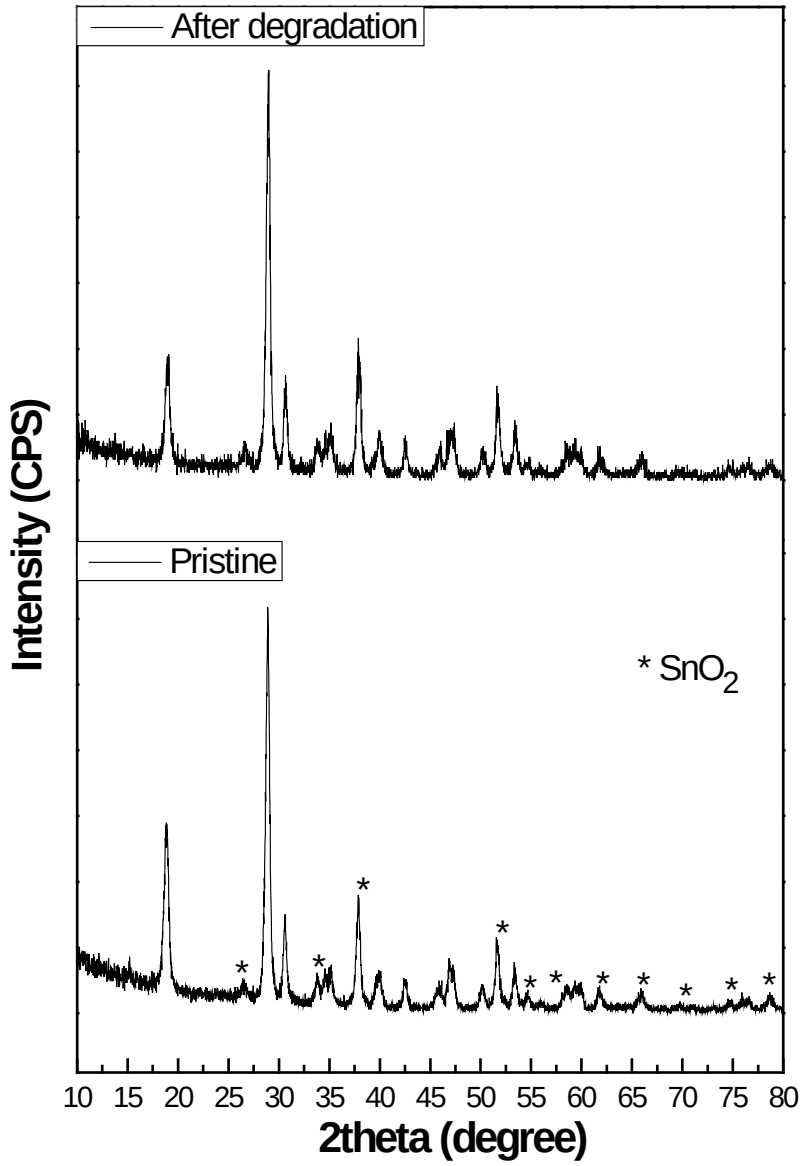

Figure S6. Gracing-incidence-angle XRD for the pristine Mo-$BiVO_4$ sample and the one after 50 h of photo-corrosion, related to Figure 4.

Note that all the peaks belong to $BiVO_4$ and SnO_2 (from FTO). The peaks labelled by asterisk belong to SnO_2 and the rest correspond to $BiVO_4$. The XRD patterns for pristine and corroded samples didn't show noticeable difference. No additional peaks were found after degradation.

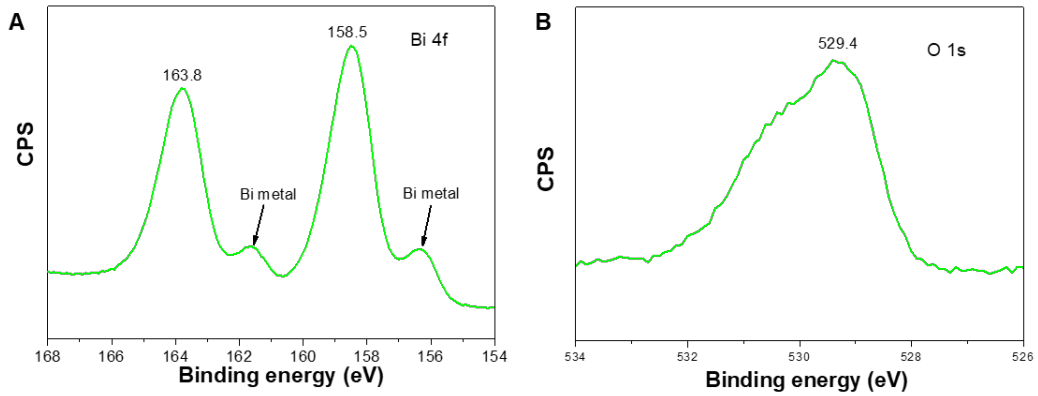

Figure S7. High resolution XPS spectra, related to Figure 4.

(A) Bi for commercial Bi_2O_3 powder. (B) O for commercial Bi_2O_3 powder.

The XPS spectrum of commercial Bi_2O_3 showed weak metallic Bi peaks also at 161.6 and 156.3 eV possibly due to contamination. Nevertheless, we could confirm the binding energies for Bi 4f orbitals in Bi_2O_3 at 163.8 and 158.5 eV. The latter are more negative to the corresponding Bi peaks of $BiVO_4$.

We refer to the XPS spectra of Bi_4O_7 reported in literature, where the respective peaks for Bi 4f7/2 and Bi 4f5/2 are located at 158.7 and 164 eV (Hu et al., 2016; Sun et al., 2017). They are also more negative to the corresponding peaks in $BiVO_4$ samples both before and after photodegradation.

Therefore, our XPS results do not contradict the possibility of Bi_2O_3 and Bi_4O_7 formation as the degradation products.

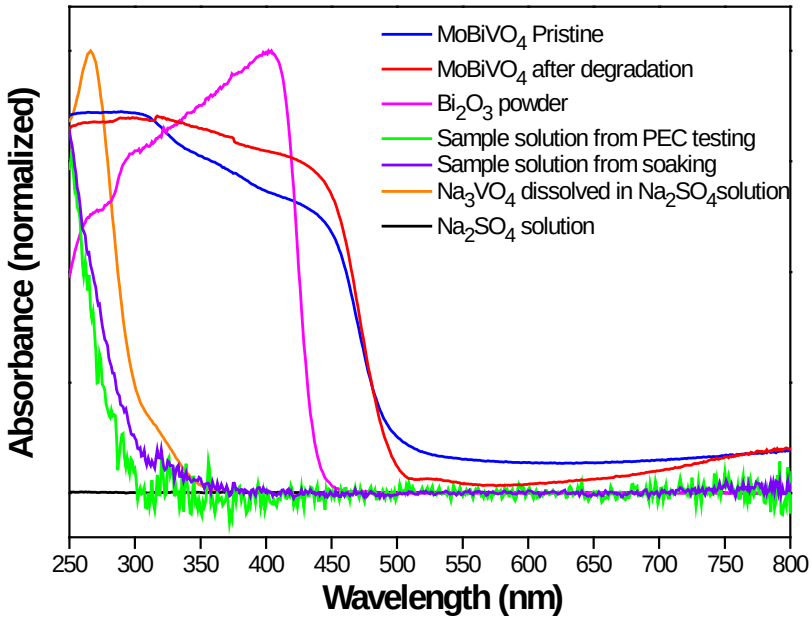

Figure S8. UV-vis spectra for various samples, related to Figure 4.

To further identify the composition of the passivation layer, we resorted to UV-vis (ultraviolet-visible) investigations. The various spectra obtained for different samples are given in Figure S8. As evident, the Mo-$BiVO_4$ photoanode after the test run showed a stronger absorbance in the range 310 – 460 nm compare to the pristine anode. This range of absorption overlaps well with that of commercial Bi_2O_3 powder also shown in the figure. The electrolyte samples after a photolysis test run, and one after just soaking in the electrolyte without photolysis, were also examine by UV-vis. Their absorbance in UV region coincides well with the spectrum obtained for a sample of VO_4^{3-} (Na_3VO_4) solution in the electrolyte. As indicated by the Pourbaix diagram, in certain degradation reactions where Bi_2O_3 and Bi_4O_7 are formed, VO_4^{3-} would also be produced. The results obtained in the UV-vis investigation also do not contradict our hypothesis that Bi_2O_3 is a possible degradation product. From literature reports, we infer that Bi_4O_7 also shows higher absorbance in 310-500 nm region than in 250-310 region (Sun et al., 2017). This also complies with our UV-vis result. Therefore, again formation of both Bi_2O_3 and Bi_4O_7 is not refuted by UV-Vis spectra.

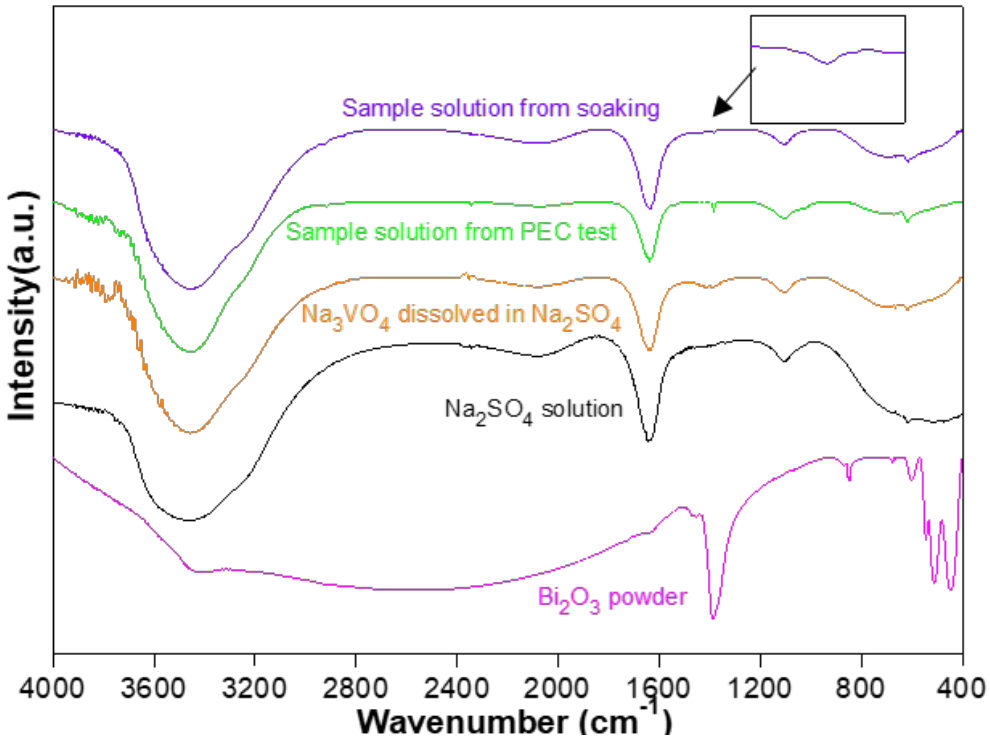

Figure S9. FTIR spectra for various samples. The inset is zoom-in on the area marked by arrow, related to Figure 4.

It is demonstrated in the FTIR (fourier-transform infrared) spectra that compared to bare Na_2SO_4 solution, the sample solution after photolysis revealed one additional response at 1384 cm^{-1}, which coincides with both Na_3VO_4 and Bi_2O_3 spectra. Since the dissolved Bi concentration in the electrolyte is very low (Bi_2O_3 is insoluble) while that of V is significantly higher, we may attribute this response to VO_4^{3-}. This further supports the possibility of the formation of $VO4^{3-}$ ions as a consequence of anode degradation.

References

Hu, Y., Li, D., Sun, F., Weng, Y., You, S., and Shao, Y. (2016). Temperature-induced phase changes in bismuth oxides and efficient photodegradation of phenol and p-chlorophenol. J Hazard Mater *301*, 362-370.

Kresse, G. (1996). Efficient iterative schemes for ab initio total-energy calculations using a plane-wave basis set. Phys Rev B *54*, 11169–11186.

Lee, D.K., and Choi, K.-S. (2017). Enhancing long-term photostability of $BiVO_4$ photoanodes for solar water splitting by tuning electrolyte composition. Nat Energy *3*, 53–60.

Persson, K.A., Waldwick, B., Lazic, P., and Ceder, G. (2012). Prediction of solid-aqueous equilibria: scheme to combine first-principles calculations of solids with experimental aqueous states. Phys Rev B *85*, 235438.

Sun, M., Wang, Y., Shao, Y., He, Y., Zeng, Q., Liang, H., Yan, T., and Du, B. (2017). Fabrication of a novel Z-scheme g-C_3N_4/Bi_4O_7 heterojunction photocatalyst with enhanced visible light-driven activity toward organic pollutants. J Colloid Interface Sci *501*, 123-132.

Toma, F.M., Cooper, J.K., Kunzelmann, V., McDowell, M.T., Yu, J., Larson, D.M., Borys, N.J., Abelyan, C., Beeman, J.W., Yu, K.M., *et al.* (2016). Mechanistic insights into chemical and photochemical transformations of bismuth vanadate photoanodes. Nat Commun *7*, 12012.

Yao, X., Wang, D., Zhao, X., Ma, S., Bassi, P.S., Yang, G., Chen, W., Chen, Z., and Sritharan, T. (2018). Scale-up of $BiVO_4$ photoanode for water splitting in a photoelectrochemical cell: issues and challenges. Energy Technol *6*, 100–109.